Synthesis and Characterization of Porous Mn_3O_4 Nanoparticles: Influence of Fuel Variation on its Structural, Electrical, Optical and Electrochemical Properties.

Premakumari P[1], Latha.H.K.E[2*], G.Nagaraju[3]

[1] Department of Electronics and communication, Government Polytechnic, Turuvekere, Tumkur-572227, Karnataka,

[2]Department of Electronics and Instrumentation Engineering. Siddaganga Institute of Technology, Tumkur -572103, Karnataka, India

[3]Department of chemistry, Siddaganga Institute of Technology, Tumkur-572103, Karnataka, India

Abstract

Owing to the fascinating facets like inexpensive, eco-friendly nature, natural abundance and its existence of manganese in a variety of oxidation states with broad application in many fields have grabbed the extensive attention for the formation of Mn_3O_4 nanoparticles. In the current work, porous Mn_3O_4 nanoparticles are prepared using green combustion synthesis (GCS) that procedure the usage of manganese nitrate tetrahydrate and Tamarind seed powder (TSP) as precursor and fuel. Present paper discusses an impact of fuel variant on properties of electrical, structural, optical and electrochemical when TSP is assorted as 0.4 g and 0.5 g to obtain samples Mn400 and Mn500 respectively. The synthesized nanoparticles of Mn_3O_4 are studied using structural (XRD, FTIR, FESEM, HRTEM and BET), electrical (UV-DRS) and electrochemical (EIS) techniques. The XRD patterns divulge that the synthesized Mn_3O_4 nanoparticles are tetragonal structured with highly crystalline in nature. The FTIR peaks found at 494 cm-1, 515 cm-1 and 603 cm-1 delineate Mn-O streching bonds. The study of FESEM images depict that the synthesized Mn_3O_4 nanoparticles are porous in nature. The HRTEM image reports d-spacing of 0.28nm for sample Mn400. The electrical (UV-DRS) analysis reports the band gap that ranges 1.375 to 1.378eV. EIS study reports impedance in the range from 142 and 176 Ω. The BET analysis affirms that sample Mn400 is having specific surface area of 2.7245 m^2 / g with Type-II isotherm classification. The prepared Mn_3O_4 nanoparticles using 0.4g fuel (Mn400) exhibits expanded properties of structural, optical, electrical and electrochemical. Hence, these nanoparticles may additionally be used in more than a few fields of utility such as rechargeable batteries, electrochemistry, air decontamination, catalysis, optical and magnetic resonance imaging, molecular adsorption, magnetism and supercapacitors.

Keywords: Manganese (II), Mn_3O_4 Nanoparticles, Porous nature, Supercapacitor;

1. Introduction:

Nanotechnology is very profound technology from past few decades since it finds multidisciplinary approached applications. In nanomaterial, it provides unpredictable results as the particle size reduces, that leads to respective changes in the properties (electrical, optical and structural) of the particle along with other material[1]. Synthesis of nanomaterial is one of the basic processes in the nanotechnology to tailor the particle properties as required. So far diverse techniques have been adopted to synthesize the nanomaterial[2] . Combustion synthesis technique is one of them and this is simple method to prepare the nanoparticle (NP) as it provides good yield and consumes less time [3-5] . Due to the worldwide increasing attention towards the environmental engineering applications, present work is concentrated on the green synthesis. This is to achieve a sustainable NP, economically viable,environmental friendly processes and accepted by the society. Therefore green combustion synthesis method is adopted to synthesize metal oxide NP due their interesting properties such as extremely small size, surface modifiability, high surface area to volume ratio, great biocompatibility and excellent magnetic properties [6-7]. Manganese oxide is promising material due to the advantages such as high specific capacitance, low-cost, high-power density and environmental friendly. It has many oxidation states like MnO_2, Mn_2O_3 and Mn_3O_4 etc., in which Mn_3O_4 is most stable and has broad applications in various fields such as rechargeable batteries, electrochemistry, air decontamination, catalysis, optical and magnetic resonance imaging, molecular adsorption, magnetism and supercapacitors and killing the cancer cells through photodynamic approach [8-10]. In this work for synthesis of Mn_3O_4 NPs, manganese nitrate is used as precursor along

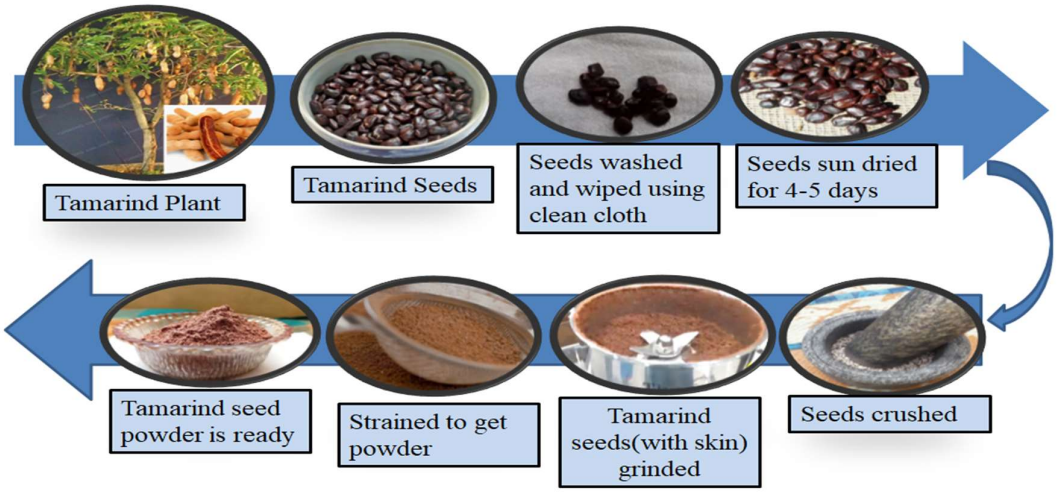

Figure 1: Preparation of TSP

with TSP as fuel. Later fuel variation is done as 0.4 g to 0.5 g, so as to obtain Mn400 and Mn500 NPs respectively. The analysis of synthesized Mn_3O_4 NPs is done by various characterization techniques such as structural (XRD, FTIR, FESEM, HRTEM and BET), optical (UV-DRS) and electrochemical (EIS).

2. Synthesis and characterization of Mn_3O_4 nanoparticles:

The chemical used in the synthesis process is procured from Vasa Scientific Co, Bangalore and used without any further purification

2.1 Preparation of fuel:

Present work uses TSP as fuel in the synthesis of manganese oxide nanoparticles. The preparation process of fuel is represented in Figure 1. The locally obtained Tamarind seeds are washed using distilled water to remove contaminations, wiped and sun dried for 3 to 4 days. Later seeds are crushed and grinded. Using strainer the TSP is strained and same is used for synthesis of manganese oxide nanoparticles.

2.2 Synthesis of Mn_3O_4 nanoparticles:

The synthesis process of manganese oxide NPs by GCS technique is depicted in Figure 2. A 1.255 g of manganese nitrate is used as precursor and the precursor weight is kept constant throughout the synthesis process. To prepare two samples, two crucibles are taken into which precursor is added along with 0.4 g and 0.5 g of TSP respectively. Later 5 ml of water is added to each crucible and mixed well using spatula until homogeneous solution is achieved. Muffle furnace is preheated in which each crucible is kept for combustion process at 500°C for 12-15 minutes. Later samples are calcinated at 700°C for 3 h. The layers of manganese oxide are formed on sides of crucible is scratched using spatula and grounded well to obtain the NPs. These samples are named as Mn400 and Mn500 respectively for 0.4 g and 0.5 g of TSP.

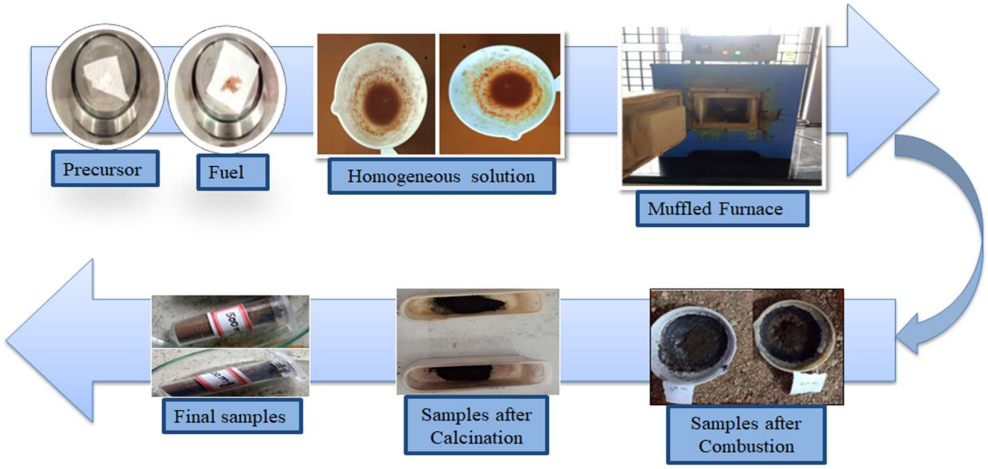

Figure 2: Preparation of Manganese oxide

2.3 Characterization of synthesized Manganese oxide nanoparticles:

Various characterization techniques (XRD, FTIR, FESEM, HRTEM, UV-DRS, EIS and BET) help to reveal the applicability of synthesized NPs for the specific applications. Smart lab RIGAKU X-ray diffractormeter that uses target as Cu Kα (λ=1.54058Å) is used for XRD analysis. FTIR analysis is carried out in the range 400 to 4000 cm^{-1} with spectral resolution of 4cm^{-1} using BRUKER ALPHA. Microstructural analysis is carried out using HITACHI SUI5IO and JEOL 2100). Optical studies are performed using Agilent technology Cary 60. Quanta Chrome Nova -1000 and Biologic SP200 is used to study BET analysis and EIS studies respectively.

3. Experimental results and discussion:

3.1 XRD Analysis:

The XRD patterns of the synthesized Mn_3O_4 NPs are shown in Figure 3. The 2θ values and the indexing plane were found to be 28.9° (1 1 2), 30.9° (2 0). 0), 32.3° (1 0 3) , 36.0° (2 1 1), 38.0° (0 0 4), 44.4° (2 2 0), 50.8° (1 0 5), 58.5° (3 2 1), 59.9° (2 2 4) and 64.6° (4 0 0). All peaks are mapped into the JCPDS number 01-080-0382, which is a Mn_3O_4 tetragonal structured NPs structure with lattice parameters a = b = 5.7650 Å and c = 9.4420 Å [11–13]. The crystal size [13], stain and dislocation density of the main XRD plane (2 1 1) for the synthesized Mn_3O_4 nanoparticles are calculated and listed in Table 1. The results show that the crystal size increased as the fuel changed from 0.4 to 0.5 g. A smaller crystal size is observed for the Mn400 sample. This increases the ratio between surface area and volume, thereby increasing surface area and energy [14]. An increase in strain and dislocation density was observed for this sample. The average crystal size was calculated from all peaks for the Mn400 and Mn500 samples and was found to be 30.972 and 36.201 nm, respectively. Therefore, an increase in the average crystal size is observed with increasing fuel change. The lattice parameters for the samples are constant, implying no disorders.

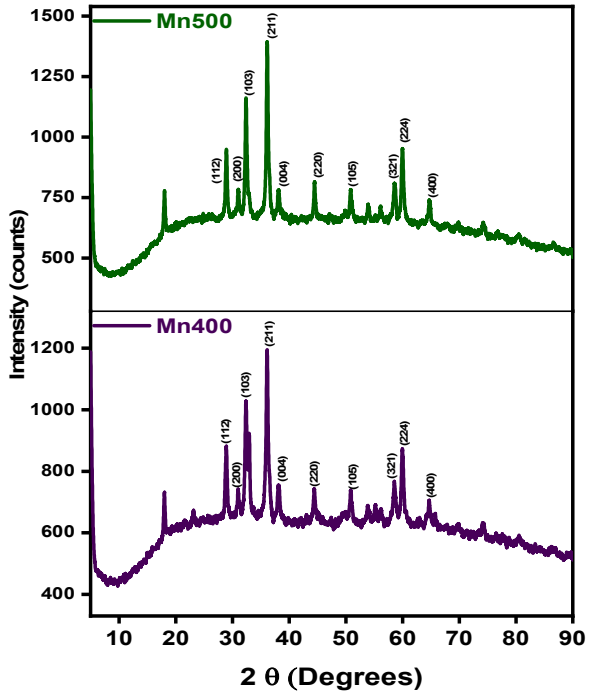

Figure 3: XRD patterns of Mn $_3O_4$ nanoparticles

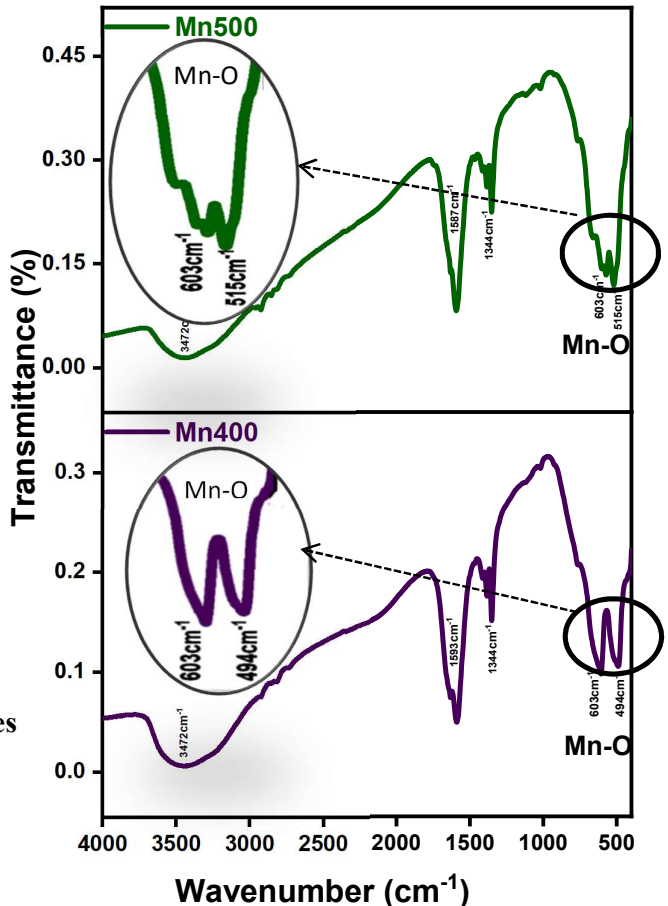

Figure 4: FTIR spectrums of *Mn_3O_4* nanoparticles

Table 1. Calculation of crystalline size, strain and dislocation density of synthesized Mn_3O_4 nanoparticles

Sample name	Peak position 2θ (Degrees)	Orientation	FWHM (β) in (Degrees)	Crystalline size in nm	Strain Є	Dislocation density δ(10^{15} lines / m^2)	Lattice parameter (Å)
Mn400	36.121	211	0.197	44.341	0.0468	50.8613	a=b=5.7650 c=9.4420
Mn500	36.123	211	0.177	45.255	0.0421	41.2189	

3.2. FTIR Analysis:

The FTIR spectra of Mn_3O_4 nanoparticle sample is represented in the Figure 4. The significant bands observed at 494 cm^{-1}, 515 cm^{-1} and 603 cm^{-1} delineates Mn-O stretching bonds. The bands observed at 1344 cm^{-1}, 1587 cm^{-1} and 1593 cm^{-1} are attributed to moisture molecule adsorption and O-H bending vibration with Mn atoms. The band observed at 3472 cm^{-1} is the O-H group, this is because of the sample pellet preparation [15-17]. It is observed that no other compound bands reported hence the formation of pure Mn_3O_4 nanoparticles is confirmed. Also, it is observed that when fuel variation is increased, it reduces the FWHM (Full width at half maxima) peak in FTIR. This is having good agreement with XRD plane (2 1 1).

3.3. FESEM:

The morphology of the synthesized Mn_3O_4 nanoparticle is studied by adopting FESEM technique. The image depicted in Figure 5 shows that the synthesized samples are porous in nature. With the increase in the fuel variation, increase in the porosity is observed. Figure 6 is the representation of elemental composition of synthesized Mn_3O_4 nanoparticles. The results revealed the presence of Mn, C and O components and its corresponding percentage are also represented (tabulated). This infers the presence of in-situ carbon (due to fuel) in the synthesized Mn_3O_4 nanoparticles.

3.4 HRTEM:

The HRTEM is carried out for the sample Mn400. The HRTEM micrograph at 100 nm and 20 nm depicted in Figure 7 (a, b) represents the porosity of synthesized Mn_3O_4 NPs. Hence HRTEM results have good agreement with the FESEM results. Figure 7b exhibits crystallite size of synthesized Mn_3O_4 NPs varies from 25.44 to 63.52 nm. From Figure 7c, d-spacing obtained is 0.28 nm which matches well with the (2 0 0) plane (XRD Figure 3). Figure 7d depicts that the synthesized Mn_3O_4 NPs are polycrystalline in nature and planes are matched with the (2 0 0), (2 2 0) and (4 0 0) orientation.

3.5. BET analysis:

By adopting the Brunauer-Emmett-Teller technique the specific surface area of the synthesized Mn_3O_4 sample and pore diameter is determined. The adsorption / desorption curve along with the pore distribution is depicted in the Figure 8. The specific surface area obtained was 2.7245 m^2/g and the pore diameter was found to be 1.29 nm. From the physisorption aspect classification on the pore size, the synthesized Mn_3O_4 nanoparticle is microporous in nature. The adsorption / desorption isotherm is matched with the Type II isotherm. As the Mn_3O_4 material is sintered at high temperature, the reduction in the specific surface area with increase in the average crystallite size is observed [18]. Therefore the BET results are in good agreement with XRD and FESEM, indicating the formation of microporous material.

3.6. UV-DRS analysis:

Diffuse reflectance spectroscopy technique is adopted to determine the optical band gap in the synthesized Mn_3O_4 nanoparticles. To calculate the band gap Kubelka munk function is used [19, 20]. The Kubelka-munk theory provides a theoretical description of the diffuse reflectance spectroscopy. When the powder sample is illuminated with light, part of the light is reflected off the powder surface and the rest penetrates the powder and disperses. When light of a certain length is absorbed by samples, measurements of diffuse reflected light at different wavelengths will give a spectrum called diffuse reflectance spectrum. The intensity of the scattered reflection spectrum in the limit case of a sample of infinite thickness is effectively expressed by the Kubelka-munk equation

$$\frac{K}{S} = \frac{(1-R)^2}{2R} \quad \ldots\ldots\ldots\ldots\ldots\ldots\ldots (1)$$

Where K = Molar absorption coefficient = $(1\text{-}R)^2$, S = Scattering factor = (2 R). R = Reflectance of material. The band gap found for Mn400 and Mn500 samples are 1.375 and 1.378 eV respectively. When the fuel is increased from 0.4 to 0.5 g, the band gap is increased as represented in Figure 9. The minimum band gap is obtained for the Mn400 sample indicating good conductivity.

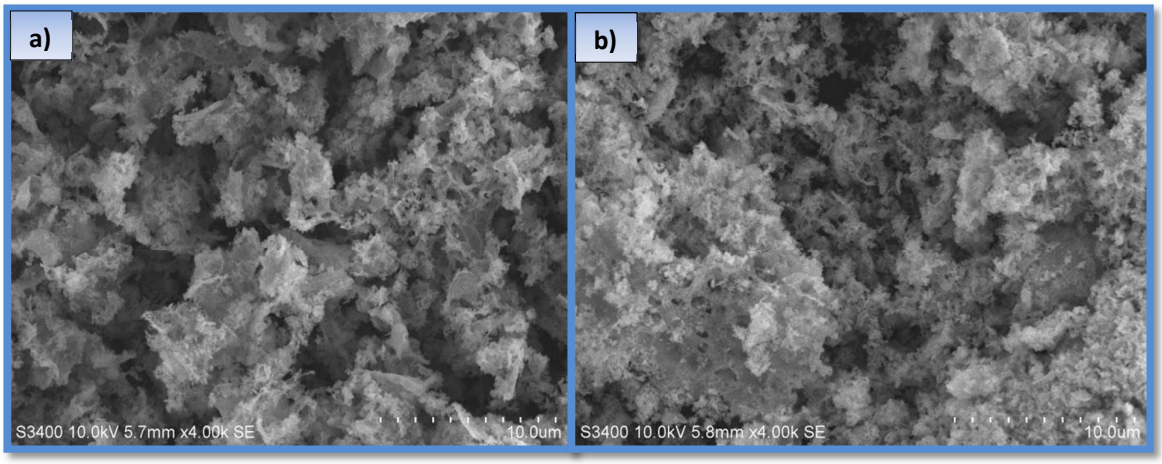

Figure 5: FESEM images of Mn_3O_4 nanoparticles a) Mn400 b) Mn500

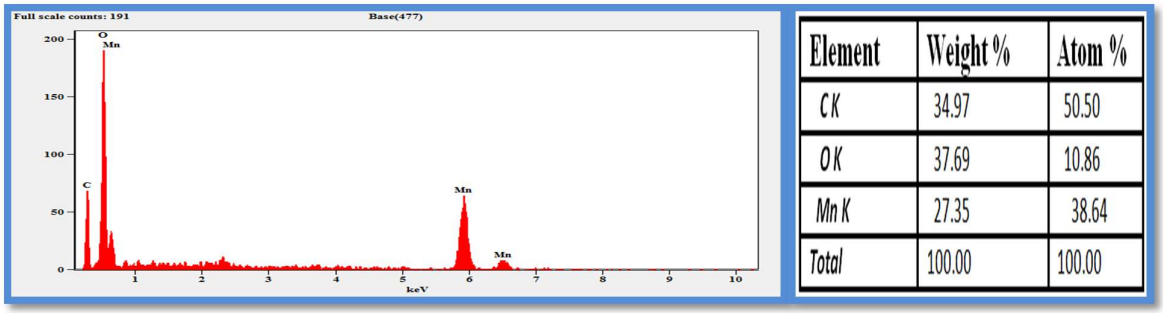

Element	Weight %	Atom %
C K	34.97	50.50
O K	37.69	10.86
Mn K	27.35	38.64
Total	100.00	100.00

Figure 6: EDAX of Mn400 sample

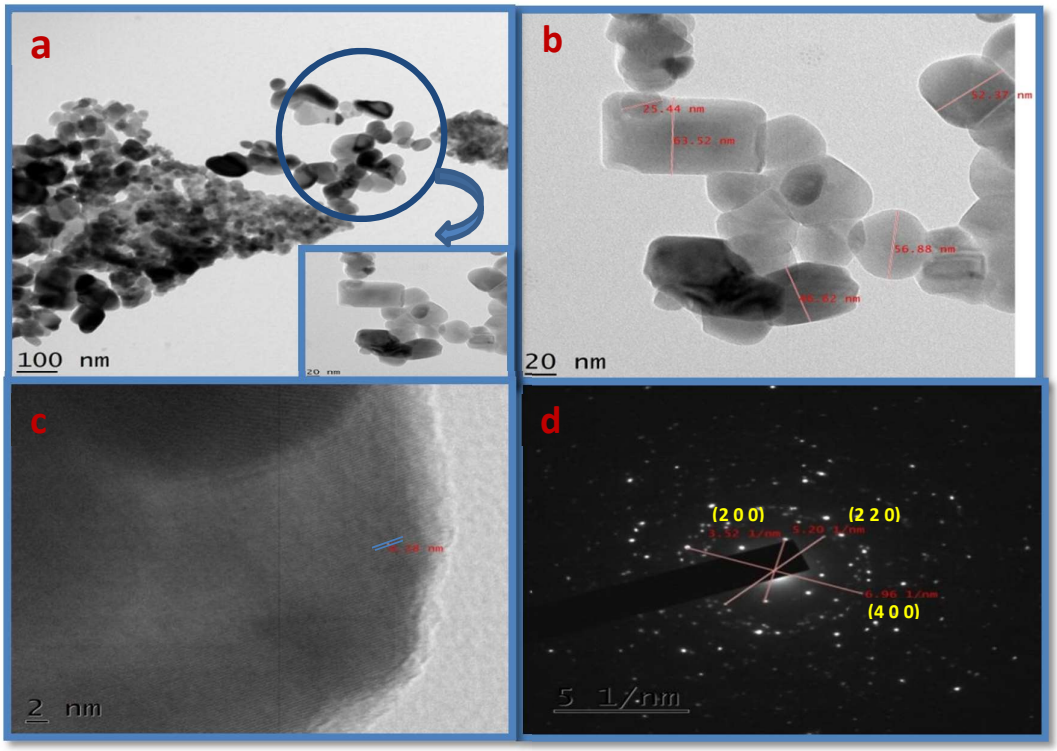

Figure 7: HRTEM images of Mn400 sample (a, b) Micrographs of Mn_3O_4 nanoparticles (c, d) SAED patterns

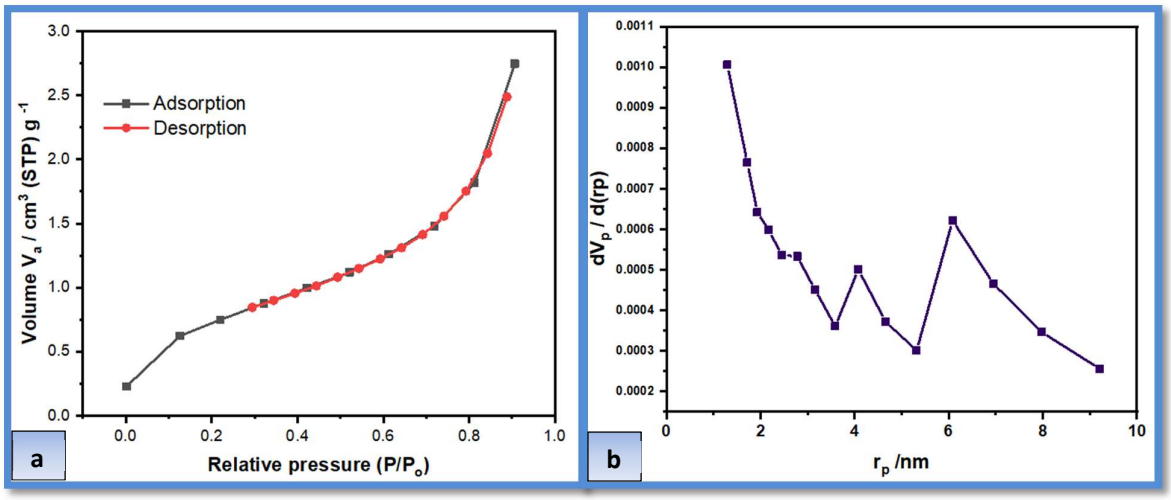

Figure 8: (a) Nitrogen adsorption / desorption isotherm (b) Pore size distribution of Mn400 sample

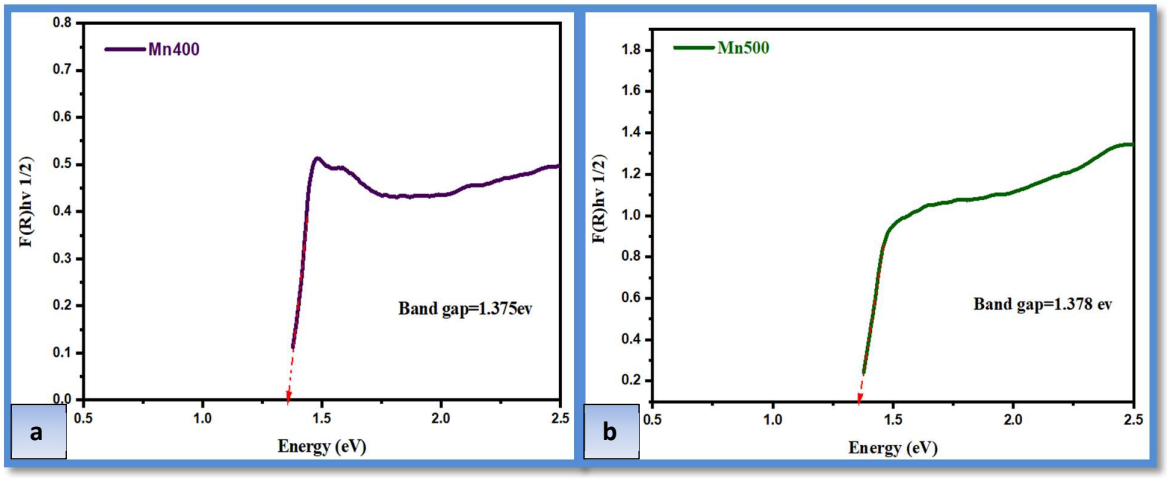

Figure 9: UVDRS Band gap representations of Mn_3O_4 nanoparticles (a) Mn400 (b) Mn500

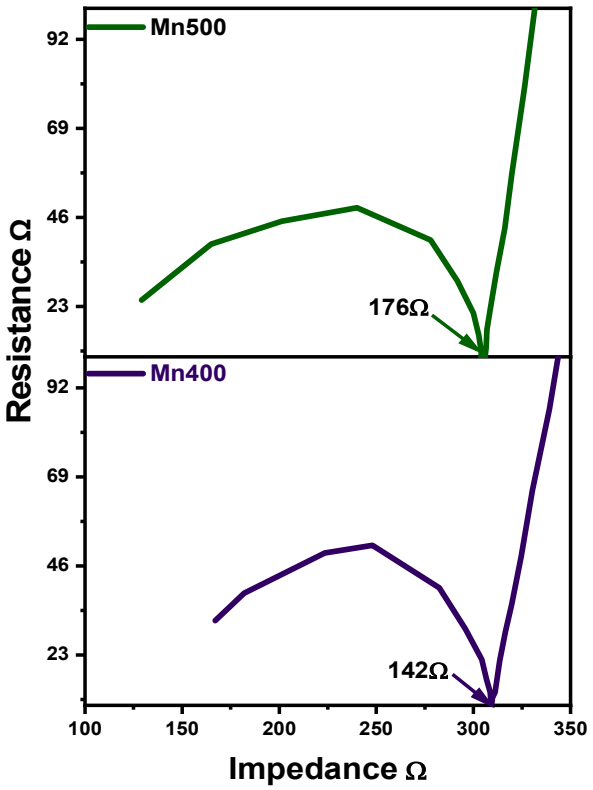

Figure 10: Nyquist plot of Mn_3O_4

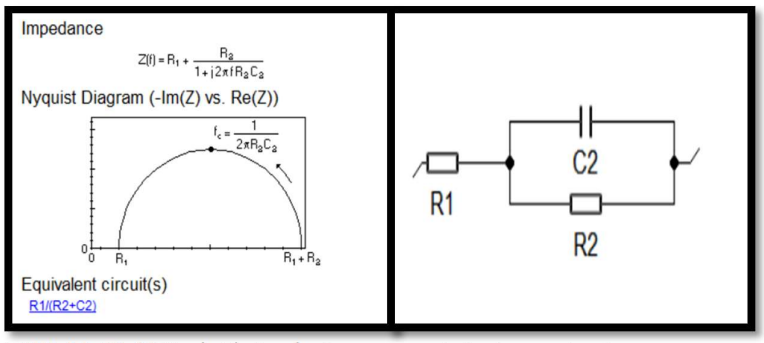

Figure 11: Nyquist impedance semicircle equivalent

Table 1: equivalent circuit component values

Component list	Component value
R1	1KΩ
R2	100Ω
C2	0.1µF

3.7. EIS analysis:

EIS analysis process has two phases. In phase1 - Using proper procedure, Glassy working electrode (One of the electrode in three electrode system) is cleaned and Sample to be analyzed is deposited on it. In Phase2 – Three electrode system is connected to the instrument (Biologic SP200) and interfaced using EC Lab software [21]. Then Nyquist plot is obtained as depicted in Figure 10. The obtained resistance for Mn400 and Mn500 samples is 142 Ω and 176 Ω respectively. It is observed from the plot that the sample Mn400 is having minimum resistance indicating good conductivity. The Z-Fit tool in EC Lab software is used on Nyquist impedance circle to obtain the corresponding equivalent circuit. The equivalent circuit and its component value are represented in Figure 11 and Table 2. Also Bode plot representation in terms of phase and magnitude for Mn400 and Mn500 samples are plotted (and is shown in Figure. 12). The Bode plot is as depicted in Figure 12. The maximum frequency (fmax) is identified from the phase plot to calculate the electron lifetime [22]. The electron lifetime for Mn400 and Mn500 samples are found as 28.8 and 39.8 ms respectively. These results are in good agreement with the EIS impedance and band gap.

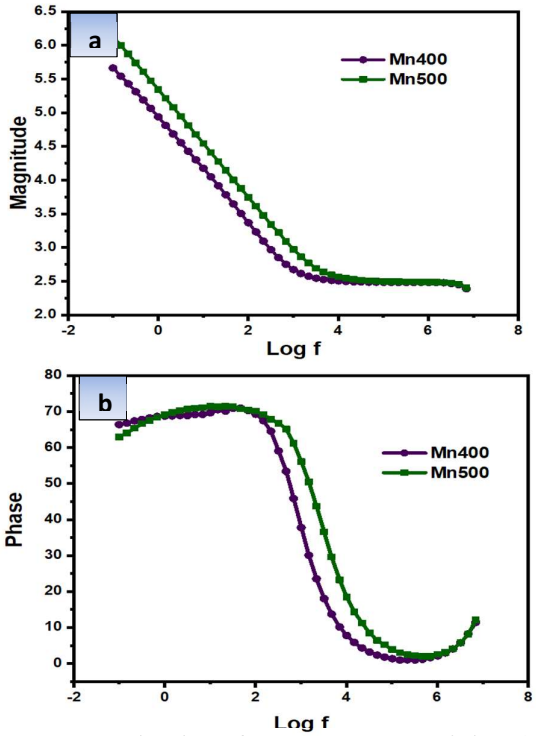

Figure 12: Bode plot of Mn_3O_4 nanoparticles a) Magnitude plot b) Phase plot

4. Conclusion

The porous Mn_3O_4 NPs are successfully synthesized by GCS technique. The influence of fuel variation on structural, optical, electrical and electrochemical properties of synthesized Mn_3O_4 nanoparticles is analyzed. The XRD and FTIR results confirm the formation of pure tetragonal structured Mn_3O_4 nanoparticles with good crystallanity. The morphological studies reveal that the synthesized material is porous in nature, having the feature of in-situ carbon. The optical study shows the lesser band gap of 1.375 eV for Mn400 sample. Also electrochemical analysis of Nyquist plot and Bode plot reports the smaller resistance of 142 Ω and lesser electron lifetimes of 28.8 ms for Mn400 sample. Mn400 sample has showed (exhibited) good electrical and electrochemical performance indicating good conductivity. Therefore, the synthesized sample (Mn400) is suitable for the battery and supercapacitors application as porous material improves the performance of the device.

5. Acknowledgement:

The authors thank Department of Physics, Siddaganga Institute of Technology, Tumkur for permitting to carryout experiments.

6. Reference

1. M. Pande and A. N. Bhaskarwar, Nanoparticles: Preparation and characterisation. 2015. (Book as a reference)
2. N. A. I. Md Ishak, S. K. Kamarudin, and S. N. Timmiati, "Green synthesis of metal and metal oxide nanoparticles via plant extracts: an overview," Mater. Res. Express, vol. 6, no. 11, 2019, doi: 10.1088/2053-1591/ab4458.
3. E. Carlos, R. Martins, E. Fortunato, and R. Branquinho, "Solution Combustion Synthesis: Towards a Sustainable Approach for Metal Oxides," Chem. - A Eur. J., vol. 26, no. 42, pp. 9099–9125, 2020, doi: 10.1002/chem.202000678.
4. G. P. Nagabhushana and G. T. Chandrappa, "Facile solution combustion synthesis of monoclinic VO2: A unique and versatile approach," J. Mater. Chem. A, vol. 1, no. 38, pp. 11539–11542, 2013, doi: 10.1039/c3ta11692a.
5. B. D. Stojanovic, A. S. Dzunuzovic, and N. I. Ilic, Review of methods for the preparation of magnetic metal oxides. Elsevier Inc., 2018.
6. S. Saif, A. Tahir, and Y. Chen, "Green synthesis of iron nanoparticles and their environmental applications and implications," Nanomaterials, vol. 6, no. 11, pp. 1–26, 2016, doi: 10.3390/nano6110209.
7. C. P. Devatha and A. K. Thalla, Green Synthesis of Nanomaterials. Elsevier Ltd., 2018.
8. D. P. M. D. Shaik, P. Rosaiah, and O. M. Hussain, "Supercapacitive properties of Mn 3 O 4 nanoparticles synthesized by hydrothermal method," Mater. Today Proc., vol. 3, no. 1, pp. 64–73, 2016, doi: 10.1016/j.matpr.2016.01.122.
9. Chunyu ZHU, Cheng-gong Han, Genki Saito and Tomohiro AKIYAMA. Facile synthesis of MnO/carbon composites by a single-step nitrate-cellulose combustionsynthesis for Li ion battery anode. Volume 689,2016,Pages 931-937,ISSN 0925-8388, https://doi.org/10.1016/j.jallcom.2016.08.054.
10. X. Zhang, Z. Yue, H. Zhang, L. Liu, and X. Zhou, "Repeated administrations of Mn 3 O 4 nanoparticles cause testis damage and fertility decrease through PPAR-signaling pathway," Nanotoxicology, vol. 14, no. 3, pp. 326–340, 2020, doi: 10.1080/17435390.2019.1695976.
11. H. E. Ali et al., "Control the nanostructured growth of manganese oxide using starch: Electrical and optical analysis," Optik (Stuttg)., vol. 227, p. 165969, 2021, doi: 10.1016/j.ijleo.2020.165969.
12. N. Mironova-Ulmane et al., "Synthesis and vibration spectroscopy of nano-sized manganese oxides," Acta Phys. Pol. A, vol. 133, no. 4, pp. 1013–1016, 2018, doi: 10.12693/APhysPolA.133.1013.
13. R. Sagar, " Structural and electrical studies of nanocrystalline Mn 3 O 4 ," Ferroelectr. Lett. Sect., vol. 45, no. 4–6, pp. 94–98, 2018, doi: 10.1080/07315171.2018.1564875
14. H. T. Phan and A. J. Haes, "What Does Nanoparticle Stability Mean?," J. Phys. Chem. C, vol. 123, no. 27, pp. 16495–16507, 2019, doi: 10.1021/acs.jpcc.9b00913.
15. H. Dhaouadi, O. Ghodbane, F. Hosni, and F. Touati, " Mn 3 O 4 Nanoparticles: Synthesis, Characterization, and Dielectric Properties ," ISRN Spectrosc., vol. 2012, pp. 1–8, 2012, doi: 10.5402/2012/706398.
16. M. Nekoeinia, S. Yousefinejad, F. Hasanpour, and M. Yousefian-Dezaki, "Highly efficient catalytic degradation of p-nitrophenol by Mn 3 O 4.CuO nanocomposite as a heterogeneous fenton-like catalyst," J. Exp. Nanosci., vol. 15, no. 1, pp. 322–336, 2020, doi: 10.1080/17458080.2020.1796977.
17. M. M. Rahman, H. M. Marwani, F. K. Algethami, and A. M. Asiri, "Comparative performance of hydrazine sensors developed with Mn 3 O 4/carbon-nanotubes, Mn 3 O 4/graphene-oxides and Mn 3 O 4/carbon-black nanocomposites," Mater. Express, vol. 7, no. 3, pp. 169–179, 2017, doi: 10.1166/mex.2017.1367.
18. O. Amadine, Y. Essamlali, A. Fihri, M. Larzek, and M. Zahouily, "Effect of calcination temperature on the structure and catalytic performance of copper-ceria mixed oxide catalysts in phenol hydroxylation," RSC Adv., vol. 7, no. 21, pp. 12586–12597, 2017, doi: 10.1039/c7ra00734e.
19. H. G. Hecht, "Interpretation of Diffuse Reflectance Spectra.," J Res Natl Bur Stand Sect A Phys Chem, vol. 80 A, no. 4, pp. 567–583, 1976, doi: 10.6028/jres.080A.056.

20. V. Džimbeg-Malčić, Ž. Barbarić-Mikočević, and K. Itrić, “kubelka-munk theory in describing optical properties of paper (II),” Teh. Vjesn, vol. 19, no. 1, pp. 191–196, 2012.
21. N. Elgrishi, K. J. Rountree, B. D. McCarthy, E. S. Rountree, T. T. Eisenhart, and J. L. Dempsey, “A Practical Beginner’s Guide to Cyclic Voltammetry,” J. Chem. Educ., vol. 95, no. 2, pp. 197–206, 2018, doi: 10.1021/acs.jchemed.7b00361.
22. X. Tang, Y. Wang, and G. Cao, “Effect of the adsorbed concentration of dye on charge recombination in dye-sensitized solar cells,” J. Electroanal. Chem., vol. 694, pp. 6–11, 2013, doi: 10.1016/j.jelechem.2013.01.036.